APPLIED SCIENCES AND ENGINEERING

Direct observation of glucose fingerprint using in vivo Raman spectroscopy

Jeon Woong Kang[1]*, Yun Sang Park[2]*, Hojun Chang[2], Woochang Lee[2], Surya Pratap Singh[1†], Wonjun Choi[1], Luis H. Galindo[1], Ramachandra R. Dasari[1], Sung Hyun Nam[2‡], Jongae Park[2], Peter T. C. So[1‡]

Noninvasive blood glucose monitoring has been a long-standing dream in diabetes management. The use of Raman spectroscopy, with its molecular specificity, has been investigated in this regard over the past decade. Previous studies reported on glucose sensing based on indirect evidence such as statistical correlation to the reference glucose concentration. However, these claims fail to demonstrate glucose Raman peaks, which has raised questions regarding the effectiveness of Raman spectroscopy for glucose sensing. Here, we demonstrate the first direct observation of glucose Raman peaks from in vivo skin. The signal intensities varied proportional to the reference glucose concentrations in three live swine glucose clamping experiments. Tracking spectral intensity based on linearity enabled accurate prospective prediction in within-subject and intersubject models. Our direct demonstration of glucose signal may quiet the long debate about whether glucose Raman spectra can be measured in vivo in transcutaneous glucose sensing.

INTRODUCTION

The importance of monitoring blood glucose cannot be overemphasized considering the increasing population of diabetics worldwide and the associated costs (*1*–*3*). However, the painful lancing process of obtaining blood drops by finger-stick hinders people from actively monitoring blood glucose levels (*4*). Several studies report that more than half of the type 1 diabetic patients do not follow the daily self-monitoring recommendation (*5*, *6*), although it is highly recommended to avoid the risk of various complications such as cardiovascular diseases, ketoacidosis, and renal failure. Noninvasive glucose monitoring has been a technology in high demand to provide people in need with pain-free, convenient, and continuous or as frequent measurements as necessary.

Over the past decades, a variety of technologies have pursued this long quest. Among many, optical spectroscopic methods have attracted a fair amount of attention (*7*–*14*). While near-infrared (NIR) absorption spectroscopy has demonstrated some potential, extracting glucose-specific features in the presence of many confounding signals from in vivo measurements has been challenging (*15*–*21*). NIR absorption features of glucose in overtone and combination bands are broad and interfere with the absorption of other chromophores in tissue. Moreover, other noise factors, such as changes in temperature and contact pressure, easily dominate weak glucose signals in in vivo experiments.

Raman spectroscopy has been recognized as a promising method. Raman spectra have distinctive spectral features specific for target molecules. Quantitative analysis for diagnostic feasibility has been reported using various biological samples such as serum, blood, tissue, and skin (*22*–*25*). For in vivo transdermal Raman spectroscopy, acquired Raman spectra contain information on glucose molecules from the interstitial fluid (ISF) underneath the epidermis layer of the skin tissue. High-throughput Raman spectroscopic instruments have been developed and validated with small-scale clinical trials of human oral glucose tolerance test (OGTT) or animal glucose clamping test (*12*, *26*–*28*). Although these reports have claimed the diagnostic capability of the Raman system optimized for transcutaneous measurement, the absence of the characteristic Raman peaks and true prospective prediction has been a contradiction to the original motivation of using Raman spectroscopy for glucose sensing. Furthermore, glucose-specific peaks in in vivo Raman spectra are very weak, subdued by strong and time-varying skin autofluorescence and associated shot noise, which make it difficult to construct good prediction models (*29*, *30*) and may lead to misinterpretation of experimental results depending on the choice of the validation method (*13*, *31*–*33*).

A recent publication presented results from a glucose clamping test on the dog subject using Raman spectroscopy (*34*). It claimed that the actual glucose signal was measured by demonstrating the similarity between the regression *b*-vector of the partial least squares (PLS) algorithm and the known Raman spectrum of glucose solution, but without presenting glucose-specific Raman peaks in the measured spectra. Considering the possibility of chance correlation in a small amount of data, without the firm evidence of the glucose-specific Raman peaks, any claim based on indirect proof could remain inconclusive and the capability of prospective prediction would be questioned.

Here, we present experimental data that may end the long debate of whether real glucose Raman peaks can be measured in vivo. We present the results of direct observation of glucose-specific Raman peaks in three swine glucose clamping experiments. The experiments were designed to allow a wide range of glucose concentrations and long integration times to obtain Raman spectra. The clamped levels of the glucose concentration were carefully controlled by infusing dextrose solution and insulin into the swine subjects. Throughout the three trials, Raman spectra were measured from the pig ears with a high optical throughput Raman system using oblique

[1]Laser Biomedical Research Center, G. R. Harrison Spectroscopy Laboratory, Massachusetts Institute of Technology, Cambridge, MA 02139, USA. [2]Mobile Healthcare Laboratory, Device and System Research Center, Samsung Advanced Institute of Technology, Samsung Electronics Co. Ltd., 130 Samsung-ro Yeongtong-gu, Suwon-si, Gyeonggi-do 16678, Republic of Korea.
*These authors contributed equally to this work as co-first authors.
†Present address: Department of Bio-sciences and Bio-engineering, Indian Institute of Technology, Dharwad, Dharwad 580011, India.
‡Corresponding author. Email: sh303.nam@samsung.com (S.H.N.); ptso@mit.edu (P.T.C.S.)

angle laser illumination. From the measured spectra, we confirm the presence of the glucose signal and linearity between intensities of the glucose Raman peaks and the reference glucose concentrations. A robust method is introduced to predict glucose concentration by taking both glucose Raman peaks and other Raman peaks related to skin components into account. The prospective prediction of glucose is investigated in single and multiple subject recordings. Last, our approach is compared with the PLS regression analysis used in a previous study (*34*).

RESULTS

Direct observation of glucose Raman peaks

Raman spectra were acquired from pig ears every 5 min for approximately 7 hours. We modeled the acquired signal as made up of four parts: glucose Raman spectrum, tissue (non-glucose) Raman spectrum, time-varying tissue background signal, and time-independent system background signal. Glucose signals vary as glucose levels are modulated during glucose clamping experiments. Non-glucose Raman spectrum mostly originates from solid skin tissue compartments such as lipids, proteins, and collagen. When measured from the same tissue location, non-glucose Raman spectrum stays relatively unchanged. By subtracting two acquired spectra with two different glucose concentrations, the glucose signal change can be highlighted.

To demonstrate the clear glucose Raman signal from tissue measurements, we calculated the subtraction spectrum between two tissue spectra with different glucose levels (G_1 and G_2) and further compared it with the Raman spectrum from a pure glucose solution. In Fig. 1A, four subtraction spectra with four glucose differences ($\Delta G = G_1 - G_2$) are plotted along with the reference Raman spectrum from the pure glucose solution. These in vivo subtraction spectra and the reference glucose solution spectrum exhibit a high degree of similarity in the Pearson correlation coefficient, $R = 0.90$ in average. One of the characteristic glucose Raman peaks appears at 1125 cm^{-1}, and its intensity increases as the glucose difference (ΔG) increases. These observations confirm that the in vivo Raman peaks originate from glucose molecules in the tissue.

While Fig. 1A shows the increasing glucose intensities from four subtraction spectra, we also observe a linear relationship between those glucose signal intensities and the corresponding glucose concentration differences during the entire measurement period. Figure 1B demonstrates the high linearity of $R = 0.95$ between the change in spectral intensity and the glucose difference (ΔG) over the entire measurement time in trial 1. The time interval between two tissue spectra was kept constant (20 min). To analyze whether the actual ranges of glucose concentration, not only the difference ΔG, affect the linearity, three different glucose ranges were marked in three colors: blue for less than 250 mg/dl, yellow between 250 and 500 mg/dl, and red for more than 500 mg/dl. The linear relationship in the range below the actual glucose concentration of 250 mg/dl, which is meaningful for most people, was maintained as $R = 0.97$ ($R = 0.96$ for the range between 250 and 500 mg/dl and $R = 0.98$ for the range over 500 mg/dl).

On the basis of the linearity between the intensity of the glucose Raman peak and the glucose concentration difference ΔG, we performed prospective prediction. Figure 1C shows the prospective prediction with $R = 0.95$ and 6.6% of the mean absolute relative difference (MARD) for trial 1. This high rate of prospective prediction is from the high linearity observed in Fig. 1B.

Band-area ratio in intraspectrum and glucose concentration prediction

In the above analyses, we were able to confirm the existence of the glucose signal in the acquired Raman spectra and the linearity of the glucose signal to the corresponding glucose concentration difference. Subtraction spectrum-based prediction requires two measurements at different times for one prediction. Our goal is to implement the proposed Raman-based glucose sensor as a wearable device in the future. The sensor will repeatedly measure Raman spectra, and glucose levels will be predicted from a series of difference spectra.

To make a prediction based on a single measurement, we examined the normalized glucose intensity, calculated as the ratio between the glucose Raman peak intensity (band) and the dominant tissue Raman peak intensity (band) in a single measurement spectrum. For the tissue Raman intensity in this study, the strongest Raman band at 1450 cm^{-1} in a spectrum was used, corresponding to the skin protein and lipid (see Fig. 2A).

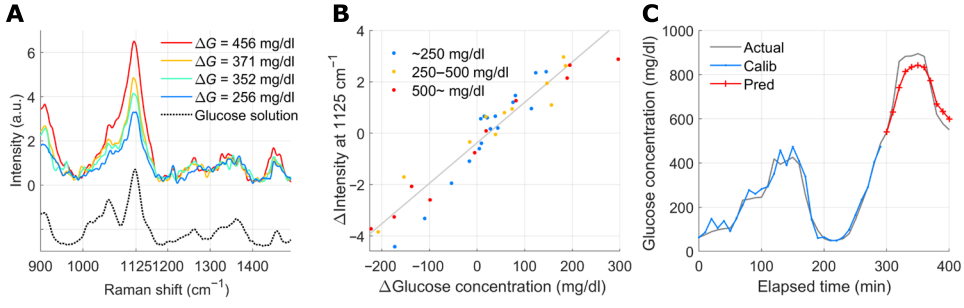

Fig. 1. Glucose Raman spectra from in vivo experiments and linearity between their spectral intensity and the corresponding blood glucose concentration. (**A**) Four subtraction spectra with four ΔG (glucose concentration difference) values. The spectra show the characteristic fingerprint, which is identical with that of aqueous glucose solution and the increase in peak intensity at 1125 cm^{-1} with the increased changes in glucose concentration. a.u., arbitrary units. (**B**) Linear relationship between the change in the Raman peak's intensity and the corresponding change in glucose concentration over the entire recording time ($R = 0.95$). The differential peak intensity is obtained by subtracting the time-moving subject-specific spectrum, lagging 20 min behind spectra to be subtracted. Three different colored dots represent three ranges of actual glucose concentration ranges: blue for lower than 250 mg/dl, yellow between 250 and 500 mg/dl, and red for 500 mg/dl and higher. The linear relationship is maintained as $R = 0.97$, 0.96, and 0.98, in the range lower than 250 mg/dl, between 250 and 500 mg/dl, and 500 mg/dl and higher, respectively. (**C**) Prospective prediction by simple linear regression based on the peak intensity change. The blue line shows the calibration result, and the red line shows the prediction result ($R = 0.95$ and MARD = 6.6% in prediction).

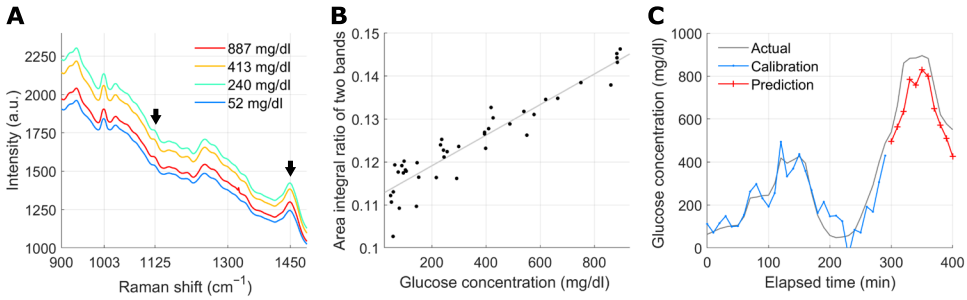

Fig. 2. The linearity between the band area ratio and glucose concentration. (**A**) Averaged spectra during each of the four clamping periods. The average glucose concentration for each clamping period is shown in the legend. The black arrows indicate the glucose Raman peak at 1125 cm^{-1} and the protein/lipid peak at 1450 cm^{-1}. (**B**) Glucose concentration versus the band area ratio corresponding to the black arrows in (A). The solid line displays the result of linear fitting ($R = 0.94$). (**C**) Prospective prediction using the band area ratio in (B) ($R = 0.94$, MARD = 13.4%).

Figure 2B demonstrates the linearity between the ratio of the two bands and the corresponding glucose concentration, $R = 0.94$. In addition, the band area ratio was analyzed for prospective prediction. In Fig. 2C, the band area ratios from approximately the first three quarters of the data were used to train a simple linear regression model, and the trained model was tested for the last untouched quarter of the data in a prospective manner. The prospective prediction based on the band area ratio resulted in $R = 0.94$ for trial 1. Extending the band area method to four selected peaks with multiple linear regression (MLR), three glucose Raman peaks at 911, 1060, and 1125 cm^{-1} and the skin component peak at 1450 cm^{-1} (see fig. S1 for details) produced the result of $R = 0.96$ for trial 1.

To check the feasibility of universal calibration using the direct glucose signal, we performed fourfold cross-validation (CV) in single-subject recordings (intrasubject CV) and leave-one-subject-out CV in multiple-subject recordings (intersubject CV; see Materials and Methods for details.). For each of the CV schemes, the suggested four band area ratios with MLR and full-range spectra with PLS regression, which has been commonly used in glucose concentration prediction, were compared. Table 1 summarized the comparison results from the intrasubject CV and intersubject CV for all the three trials.

Both the suggested band area method and the conventional full-range spectrum method show a high prediction rate in the intrasubject CV ($R = 0.85$ and 0.94 in average in all the three trials, respectively). For the intersubject CV or universal calibration, the band area approach produce a higher prediction rate ($R = 0.91$) than the conventional approach ($R = 0.62$), indicating that the direct glucose signal–based prediction can be more robust than the statistical prediction. In particular, the improved trend tracking capability was observed for trial 3: The tracking capability was improved from $R = 0.17$ in PLS regression with full-range spectra to $R = 0.88$ in MLR with four band area features, as shown in Fig. 3 (A and B).

A close examination on the data in trial 3 suggests that there might be a couple of events of disturbance during the measurement. In Fig. 3C, despite no linear correlation for the whole data, we can still observe linearity for partial recordings. From the observation, it is reasonable to assume that external perturbations, probably the movement of the subject, caused abrupt changes in the background and Raman collection efficiency. These changes can be corrected better with the four selected band area features. This effect is well displayed in Fig. 3D with the improved linearity of $R = 0.73$. Considering that statistical learning approaches, such as PLS regression, can produce desirable outputs when similar patterns accumulate, training with full-range spectra from trials 1 and 2 may not well explain the broken linearity in full-range spectra from trial 3 in the PLS regression–based full-range spectrum method.

Table 1. Results from fourfold cross-validation in single-subject recordings (intrasubject CV) and from leave-one-subject-out cross-validation with multiple-subject recordings (intersubject CV). MLR with four band area features and PLS regression with full-range spectra were used. CEG, consensus error grid.

	Band-area feature		Full-range spectrum	
	R	CEGA+B(%)	*R*	CEGA+B(%)
A. Intrasubject CV				
Trial 1	0.97	85.4	0.98	92.7
Trial 2	0.93	100.0	0.95	100.0
Trial 3	0.65	83.0	0.87	85.1
Average	0.85	89.4	0.94	92.6
B. Intersubject CV				
Trial 1	0.95	51.2	0.87	58.5
Trial 2	0.90	84.1	0.83	0.0
Trial 3	0.88	83.0	0.17	27.7
Average	0.91	72.8	0.62	28.7

System characterization

Multiple Raman instruments have been developed and tested for blood glucose monitoring in vivo. A free-space Raman spectroscopy system in reflection geometry collected the signal from human forearm using a paraboloidal mirror combined with f/1.8 spectrograph and a tall detector (*12*). However, its in-line geometry admitted unwanted Rayleigh light reflected from the tissue surface. The free-space tissue interface was also prone to the subject movement. A transmission Raman instrument with a nonimaging optical element has been used to harvest most Raman photons emerging from the tissue (*26*). A compound hyperbolic concentrator at the tissue interface effectively collected Raman photons from large solid angle. In contrast, transmission measurements from the thenar fold require a contact interface, which pinches the tissue and changes its properties during the long-term

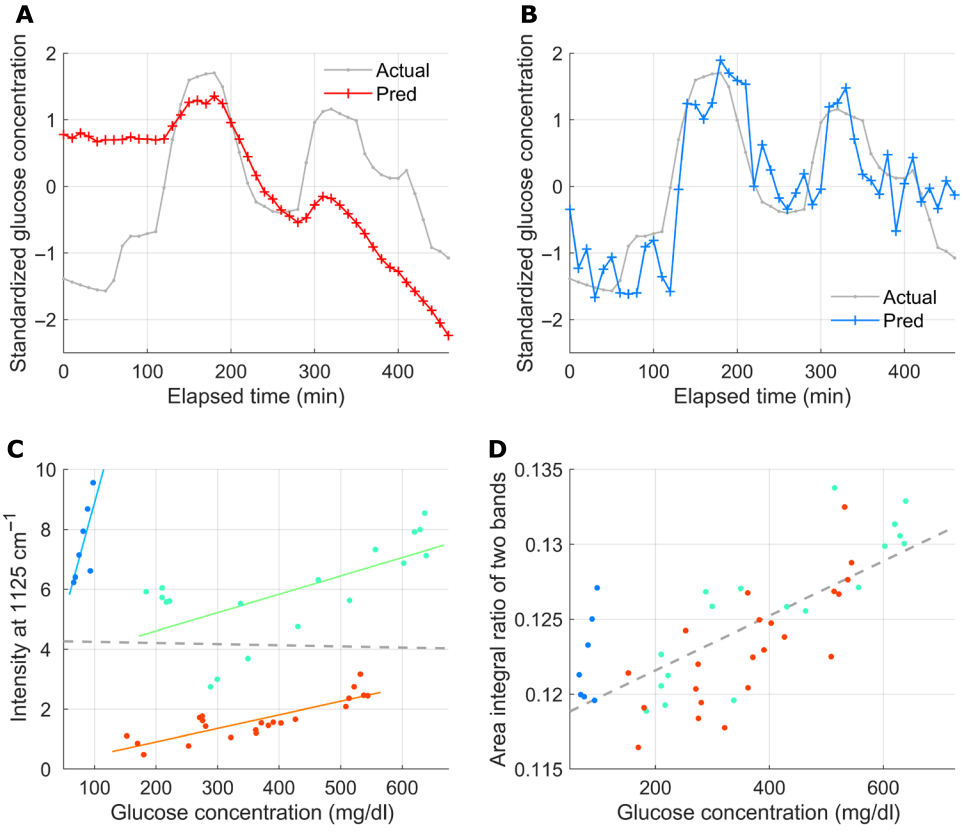

Fig. 3. Prediction in intersubject recordings. A model is trained with recordings of trials 1 and 2 and is used for prediction in trial 3 recordings. (**A**) Prediction using PLS regression with full-range background-subtracted spectra ($R = 0.17$). (**B**) Prediction using MLR with four band area features. Three are extracted from the glucose-specific bands, and the last one is from a skin component peak ($R = 0.82$). (**C**) Linearity between the Raman peak intensity and glucose concentration for trial 3 is observed only in each of the three time-continuous parts of the recordings (separated by color, $R = 0.74$ on average), but not for the entire recording ($R = -0.02$) with the spectra subtraction method. (**D**) The linearity improves with the same recordings as in (C) when the ratio of the two band area features is used ($R = 0.73$).

measurement. More recently, optical fiber probe–based Raman instrument was used (*35*). Along with a custom-designed tissue interface, it was able to reliably measure the Raman signal from the same tissue spot under the room light. However, the focused radiance of laser from one excitation fiber limits the sampling volume, and a small tip of the Raman probe presses the skin over hours of measurement, which might prevent glucose-containing ISF from circulating across the sampling volume. It is common to observe a pressure mark on soft samples after using this type of probe.

To overcome these limitations from previous instruments and directly obtain glucose Raman peaks, an off-axis Raman instrument was developed to maximize the effective sampling volume while maintaining noncontact stable long-term measurements. To investigate the benefits of this approach, we simulated how much volume is sampled for the Raman scattered light and what the fraction of total laser illumination contributed to Raman collection from a certain depth of the skin tissue. Figure 4 shows radiance distribution over the sampling volume collected by two different types of Raman probes. Radiance distribution is overlaid on the hematoxylin and eosin–stained histology images of the pig ear tissue. Both configurations show radiance distribution over 1 mm depth from the surface of skin.

The effective sampling volume under oblique angle laser illumination is shown in Fig. 4A. It gives better-spread laser radiance over the dermis layer, where ISF containing glucose molecules is considered to be distributed. The closer a sampled voxel is to the fiber bundle, the more chance it may contribute to the Raman signal. Figure 4B shows a more focused distribution of radiance over the target, representing the result of a conventional endoscope-type Raman probe contacted to skin (*35*). It shows more focused distribution of radiance over the smaller sampling volume as expected. Figure 4C presents the ratio of voxels at a given depth to all voxels illuminated over a certain threshold of radiance. At the dermis layer close to the fiber bundle, more voxels contribute to Raman scattering under the oblique angle illumination than the normal illumination through a fiber. From this perspective, the oblique angle incidence of laser can be a more effective strategy than the normal incidence to extract glucose Raman signal.

Limit of detection

To verify our analyses with the optical system, we examined the estimation of the limit of detection (LoD) of our system by the following two approaches. The first was based on linear regression. If the instrument response y is linearly related to concentration x as $y = a + b{\cdot}x$, LoD is defined as $3SD_a/b$, where SD_a is the standard deviation of y residuals and b is the slope of the linear curve [sensitivity; (*36*)]. Figure S2 shows the spectrum intensity versus the corresponding glucose concentration during the time period when fluorescence

stayed relatively flat (see Fig. 5C). Using the above LoD definition with minimal glucose concentrations around 52 mg/dl, the LoD of our measurements was calculated as ~75 mg/dl.

We also investigated the minimal glucose concentration at which the corresponding spectrum can appear above the noise level. This approach used the correlation coefficient between the glucose solution spectrum and subtraction spectra, similar to the method used in Fig. 1A. Figure S3 shows the correlation coefficient trace during the time period used in the first analysis. Glucose signal differences in subtracted spectra were observed to be buried below the noise level when the corresponding glucose concentration differences were smaller than 29 mg/dl. At the glucose concentration difference of 78 mg/dl, a distinguishing correlation coefficient from the previous data started to be observed. Although we could not determine the exact value due to the limited data points from in vivo experiment, the minimum detectable concentration was estimated to be between 29 and 78 mg/dl.

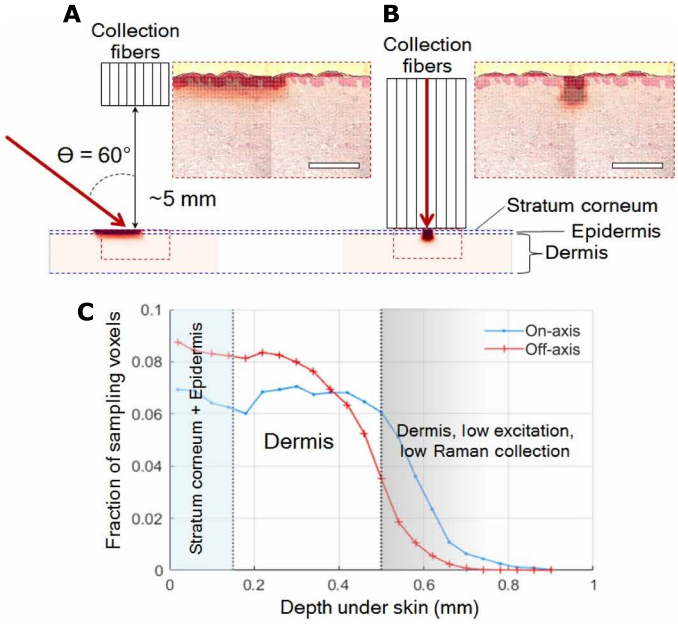

Fig. 4. Off-axis Raman excitation and collection configuration. (**A**) Radiance distribution of 830-nm laser in skin model with a configuration of the oblique angle (off-axis) laser illumination. Scale bar, 500 μm. (**B**) Radiance distribution of 830-nm laser in the same skin model when a conventional probe (on-axis) is applied (the same scale bar applied). (**C**) Fraction of sampling voxels in off-axis and on-axis configuration as a function of depth in the confined region.

DISCUSSION

The main claim of this study is the identification of glucose fingerprint peaks in in vivo transcutaneous Raman measurements. We expect that the identification of glucose fingerprint peaks in this study and the observation of their linear changes with the corresponding glucose levels could resolve the long-standing ambiguity about whether Raman system can catch glucose signal in transcutaneous glucose sensing. This was mainly enabled by the illumination collection geometry to control over the sampling volume using the noncontact off-axis system. The proposed noncontact off-axis system minimized the instability of the probe by illuminating a relatively large tissue under custom-designed large collection fiber bundles. The off-axis illumination and vertical collection geometry spatially filter out the specular Rayleigh reflection from the skin surface, and this can reduce the burden of the Rayleigh rejection filter at the probe tip. In addition, the noncontact measurement is free from potential distortions of tissue, which is important for stable long-term measurement.

In addition to the identification of glucose fingerprint peaks, prospective prediction in single-subject recordings and prediction in intrasubject and intersubject CV approaches were investigated. One important aspect in the prediction investigation was that the analysis was performed on experiments with complex blood glucose time profiles. Many previous studies on noninvasive glucose sensing have claimed their possibility on glucose concentration prediction but based on relatively simple blood glucose time profiles, such as the one on the OGTT with a monotonic increase and decrease in glucose concentration (*37*). However, training and testing regression with simple blood glucose time profiles could misdirect the regression analysis, yielding overly optimistic predictions without actual glucose sensing. Statistical learning regression modeling, such as neural network regression, could produce high prediction rate when it captures, for example, an erroneous relationship between a certain non-glucose–related artifact and measurement time that is highly correlated with glucose concentration profiles, especially in simple ones.

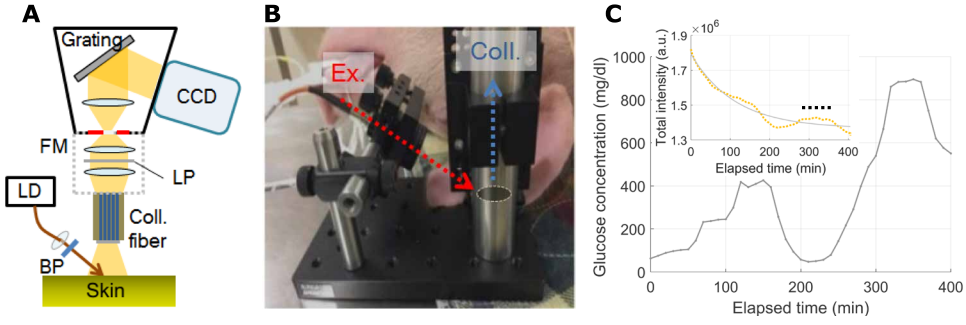

Fig. 5. Raman spectroscopy system, actual probe setup with a subject, and glucose profile during experiment. (**A**) Schematic diagram of Raman spectroscopy system for in vivo animal (swine) skin measurement. FM, *f* number matcher; LP, longpass filter; LD, laser diode; BP, bandpass filter. (**B**) Photograph of Raman probe setup with oblique illumination and vertical collection equipped on top of an anesthetized pig (photo credit: Jeon Woong Kang, MIT). (**C**) Glucose profile during the glucose clamping experiment in trial 1. Exponential time decay of fluorescence from the skin in the inset (spectrum wavelength integration; actual data in the yellow dotted line and its exponential approximation in the gray line). The dotted black line in the inset indicates the time period during which fluorescence stays nearly flat.

As the acquired signals in our experiments consist of four different Raman and background signals (see Results for details), the following sources for signal variation can be considered. The largest signal variation came from the time decay of autofluorescence in the in vivo skin tissue. In addition, movement artifacts from the in vivo subject, even under the anesthetic state, can be another great source. When the laser-targeted spot on the skin moved, the field of view of the Raman probe changed and this led to different levels of photobleaching. As the non-glucose tissue Raman spectrum, physiological changes in skin tissue during the experiment, such as sweating, may affect signal variation. Physiological vital signs from the in vivo subjects, such as body temperature and heart rate, may influence the signal variation, but there was no significant correlation found in this study between the intensity of the glucose fingerprint peak at 1125 cm^{-1} (or glucose concentration) and any of the vital signs (see fig. S4). In particular, to reduce the effect of body temperature on our experiments, such as changing the sampling volume, we used a circulating water blanket to maintain the subject's body temperature as stable as possible.

The use of the intraspectrum band area ratio was intended to track normalized changes in glucose Raman bands using a strong band from a skin component in the same spectrum. For example, when the location of the probe or its distance to skin changes due to the subject's movement, it immediately causes a change in the intensity of the measured peaks in general. Such a change may be reflected in the entire Raman signal, including glucose Raman peaks and other skin component Raman peaks. The use of the band area ratio between the two selected bands may reduce influences of those measurement artifacts on glucose Raman peaks by the intraspectrum band normalization (see Fig. 3, C and D). In this sense, the band area ratio approach can be valid, although the signal origins of glucose fingerprint peaks and protein/lipid peak differ.

To bring the Raman-based blood glucose monitoring technology to people with diabetes, challenges still remain for further developments: for example, lowering the maximum glucose concentration in experiments, reducing the integration time, miniaturizing the system, and testing with many human subjects, including people with diabetes and with different skin colors. Improving the Raman system and developing sophisticated prediction algorithms will be our future work, and the work we presented here will be a solid basis for further improvements.

MATERIALS AND METHODS

Experimental protocol

The animal experiment protocol was approved by the Massachusetts Institute of Technology (MIT) Committee on Animal Care (protocol no. 0417-033-20). Considering their anatomical and biochemical similarities with humans, three female Yorkshire pigs (40 to 55 kg) were selected for the glucose clamping test. The subjects were anesthetized under 2% isoflurane supplied via a controlled vaporizer after sedation with Telazol (5 mg/kg) and xylazine (2 mg/kg) intramuscularly and given atropine (0.04 mg/kg). The anesthesia and vital signal monitoring of the animal were performed by veterinary staffs of the MIT Division of Comparative Medicine. Two femoral vein catheters were placed in each leg aseptically for the delivery of intravenous fluids, glucose, and repeated bleeds followed by flushing of heparinized saline (10 U/ml) between blood draws. The body temperature of swine was maintained on heated table and water-circulating blankets. We examined vital signs including body temperature (see fig. S4) and found no significant correlation between body temperature and glucose levels.

The blood glucose level was modulated within the range from 52 to 914 mg/dl by infusing 30% dextrose and insulin (0.8 U/ml) for a period of 30 to 60 min at each level. Blood samples (3 ml) were drawn every 5 min from another catheter and were analyzed using a glucose analyzer (YSI 2300, YSI Inc., OH, USA). After the measurements, the ear tissue (~1 cm^2) containing the laser beam spot (~1.6 mm^2) was collected for histological analysis. No substantial change in the irradiated skin regions was observed under the selected power level for spectrum measurement. In the experiments, the animal was euthanized with pentobarbital (100 mg/kg; intravenous administration of Fatal-Plus). Clamping level profiles were designed to have maximum modulation and to avoid monotonic increases or decreases in the reference glucose concentration as well as similar patterns between subjects, while considering clinical constraints, such as time available for the session, and the recommended infusion rate depending on the subject's weight.

Instrumentation

A portable Raman spectroscopy instrument was built with an 830-nm diode laser (PI-EC-830-500-FC, Process Instruments, UT, USA), an imaging spectrograph (LS785, Princeton Instruments, NJ, USA), and a charge-coupled device (CCD; PIXIS1024BRX, Princeton Instruments, NJ, USA). The illumination collection geometry using oblique angle (off-axis) incidence of laser and noncontact vertical Raman collection was determined for the increased effective sampling volume of the targeted layer while reducing the collection of background signals.

A filtered laser beam of 250 mW was focused on the ear skin with an incidence angle of 60°, forming an elliptical beam of 1 mm × 2 mm. Light emission from the measurement spot of the skin surface was collected with a custom-made, round-to-linear optical fiber bundle consisting of 61 fibers (LEONI Fiber Optics Inc., VA, USA) to fully cover the CCD height. The fibers were custom-drawn (200 μm core diameter, Fiberguide Industries) to minimize fiber background signal. The diameter of the fiber bundle was 2 mm at the probe tip with a custom filter (Alluxa, CA, USA) attached to reject Rayleigh light. A mechanical shutter was installed inside of the spectrograph to minimize vertical pixel smearing. A full-frame image of the CCD for 285 s was consecutively acquired every 5 min with the help of Lightfield software (Princeton Instruments, NJ, USA).

Spectral data analysis

Because the high-throughput system equipped with the large-area CCD caused an image curvature of the spectrum, we performed image curvature correction for conversion from the frame image to spectrum. Two consecutive spectra, collected 5 min apart, were averaged into one 10-min-long spectrum, and Savitzky-Golay filtering (*38*) was applied to smoothen the spectrum. The analysis in this study was based on either background-removed spectra in the range of 810 to 1650 cm^{-1} by polynomial baseline subtraction (*39*) or band area features. Band area features were computed as area integral under a background-subtracted spectrum in the selected four bands: three glucose fingerprint bands at 911, 1060, and 1125 cm^{-1} and one band at 1450 cm^{-1} for proteins and lipids of the skin (see fig. S1 for details).

Linear regression analysis was performed to train and test a mapping function from spectra or band area features to corresponding glucose concentrations for calibration and prediction, respectively.

We used simple linear regression analysis for single spectrum intensities or single band area ratios, MLR analysis for four band area features, and PLS regression analysis for full-range background-subtracted spectra. For hold-out prospective prediction, all the parameters were calibrated with training samples only. We also used other validation schemes: fourfold CV in single-subject recordings, called intrasubject CV in this study, and leave-one-subject-out CV in all the three subjects' recordings, called intersubject CV. In the fourfold CV, single-subject recordings were split into approximately equally long and time-continuous partial recordings. Each of the time-continuous partial recordings was tested by a linear regression model trained with the other three time-continuous partial recordings. In the leave-one-subject-out CV, single-subject recordings were tested by a model trained with the other two subjects' recordings. In our CV schemes, all the recordings were tested once.

To quantify prediction performance with samples for testing, we calculated the Pearson correlation coefficient R between actual and predicted glucose concentrations, and the percentage of samples marked in regions A and B in the consensus error grid. MATLAB (MathWorks, MA, USA) was used for data analysis.

Simulating sampling volume

The advantages of the selected configuration were investigated with the ray-tracing simulation over a multilayered skin model (OpticStudio 15.5, Zemax, WA, USA). The Henyey-Greenstein phase function was used to numerically simulate light scattering in the tissue, with optical coefficients (μ_s, μ_a, g, and n) set differently for each layer, similar to the known human case (*40*). The number of voxels was approximately 11,000 and 4200 for oblique angle and normal laser illumination, respectively. More voxels were eligible for the collection of the Raman signal under the oblique angle configuration.

SUPPLEMENTARY MATERIALS

Supplementary material for this article is available at http://advances.sciencemag.org/cgi/content/full/6/4/eaay5206/DC1

Fig. S1. Band area feature.
Fig. S2. Estimation of the LoD using a linear regression.
Fig. S3. Analysis of the validity of calibration using the background subtraction method used in Fig. 1A and the LoD measurement.
Fig. S4. Change in glucose concentration measured by a YSI glucose analyzer and Accu-Chek finger-prickers (top panels) and vital signs from the subject.
Fig. S5. Linear regression with full-range spectra.
Fig. S6. Raman probe design.
Fig. S7. Glucose signal change corresponding to several ΔG values in glucose solution.
Fig. S8. Spectra and time course results from the band area features in MLR analysis from all the three trials.
Fig. S9. Raman intensity changes with different glucose values.

REFERENCES AND NOTES

1. K. Ogurtsova, J. D. da Rocha Fernandes, Y. Huang, U. Linnenkamp, L. Guariguata, N. H. Cho, D. Cavan, J. E. Shaw, L. E. Makaroff, IDF diabetes atlas: Global estimates for the prevalence of diabetes for 2015 and 2040. *Diabetes Res. Clin. Pract.* **128**, 40–50 (2017).
2. J. K. Kirk, J. Stegner, Self-monitoring of blood glucose: Practical aspects. *J. Diabetes Sci. Technol.* **4**, 435–439 (2010).
3. E. Renard, Monitoring glycemic control: The importance of self-monitoring of blood glucose. *Am. J. Med.* **118**, 12S–19S (2005).
4. L. Heinemann, Finger pricking and pain: A never ending story. *J. Diabetes Sci. Technol.* **2**, 919–921 (2008).
5. A. J. Karter, A. Ferrara, J. A. Darbinian, L. M. Ackerson, J. V. Selby, Self-monitoring of blood glucose: Language and financial barriers in a managed care population with diabetes. *Diabetes Care* **23**, 477–483 (2000).
6. S. R. Patton, Adherence to glycemic monitoring in diabetes. *J. Diabetes Sci. Technol.* **9**, 668–675 (2015).
7. J. T. Olesberg, L. Liu, V. V. Zee, M. A. Arnold, In vivo near-infrared spectroscopy of rat skin tissue with varying blood glucose levels. *Anal. Chem.* **78**, 215–223 (2006).
8. K. Maruo, Y. Yamada, Near-infrared noninvasive blood glucose prediction without using multivariate analyses: Introduction of imaginary spectra due to scattering change in the skin. *J. Biomed. Opt.* **20**, 047003 (2015).
9. S. Liakat, K. A. Bors, L. Xu, C. M. Woods, J. Doyle, C. F. Gmachl, Noninvasive in vivo glucose sensing on human subjects using mid-infrared light. *Biomed. Opt. Express* **5**, 2397–2404 (2014).
10. T. J. Allen, B. T. Cox, P. C. Beard, Generating photoacoustic signals using high-peak power pulsed laser diodes, in *Photons Plus Ultrasound: Imaging and Sensing 2005: The Sixth Conference on Biomedical Thermoacoustics, Optoacoustics, and Acousto-optics*, San Jose, CA, 25 April 2005.
11. J. Y. Sim, C.-G. Ahn, E.-J. Jeong, B. K. Kim, In vivo microscopic photoacoustic spectroscopy for non-invasive glucose monitoring invulnerable to skin secretion products. *Sci. Rep.* **8**, 1059 (2018).
12. A. M. K. Enejder, T. G. Scecina, J. Oh, M. Hunter, W. C. Shih, S. Sasic, G. L. Horowitz, M. S. Feld, Raman spectroscopy for noninvasive glucose measurements. *J. Biomed. Opt.* **10**, 031114 (2005).
13. M. J. Scholtes-Timmerman, S. Bijlsma, M. J. Fokkert, R. Slingerland, S. J. F. van Veen, Raman spectroscopy as a promising tool for noninvasive point-of-care glucose monitoring. *J. Diabetes Sci. Technol.* **8**, 974–979 (2014).
14. S. M. Lundsgaard-Nielsen, A. Pors, S. O. Banke, J. E. Henriksen, D. K. Hepp, A. Weber, Critical-depth Raman spectroscopy enables home-use non-invasive glucose monitoring. *PLOS ONE* **13**, e0197134 (2018).
15. O. S. Khalil, Non-invasive glucose measurement technologies: An update from 1999 to the dawn of the new millennium. *Diabetes Technol. Ther.* **6**, 660–697 (2004).
16. M. A. Arnold, G. W. Small, Noninvasive glucose sensing. *Anal. Chem.* **77**, 5429–5439 (2005).
17. K. Maruo, M. Tsurugi, J. Chin, T. Ota, H. Arimoto, Y. Yamada, M. Tamura, M. Ishii, Y. Ozaki, Noninvasive blood glucose assay using a newly developed near-infrared system. *IEEE J. Sel. Top. Quantum Electron.* **9**, 322–330 (2003).
18. K. Xu, Q. Qiu, J. Jiang, X. Yang, Non-invasive glucose sensing with near-infrared spectroscopy enhanced by optical measurement conditions reproduction technique. *Opt. Lasers Eng.* **43**, 1096–1106 (2005).
19. X. Zhang, J. H. Yeo, Temperature influence on non-invasive blood glucose measurement, in *Optical Diagnostics and Sensing IX*, San Jose, CA, 20 February 2009.
20. J. Yadav, A. Rani, V. Singh, B. M. Murari, Near-infrared LED based non-invasive blood glucose sensor, in *2014 International Conference on Signal Processing and Integrated Networks (SPIN)*, Noida, India, 20 to 21 February 2014.
21. J. Yadav, A. Rani, V. Singh, B. M. Murari, Prospects and limitations of non-invasive blood glucose monitoring using near-infrared spectroscopy. *Biomed. Signal Process Control* **18**, 214–227 (2015).
22. A. Sahu, S. Sawant, H. Mamgain, C. M. Krishna, Raman spectroscopy of serum: An exploratory study for detection of oral cancers. *Analyst* **138**, 4161–4174 (2013).
23. A. J. Berger, T.-W. Koo, I. Itzkan, G. Horowitz, M. S. Feld, Multicomponent blood analysis by near-infrared Raman spectroscopy. *Appl. Opt.* **38**, 2916–2926 (1999).
24. Y. Ozeki, W. Umemura, Y. Otsuka, S. Satoh, H. Hashimoto, K. Sumimura, N. Nishizawa, K. Fukui, K. Itoh, High-speed molecular spectral imaging of tissue with stimulated Raman scattering. *Nat. Photonics* **6**, 845–851 (2012).
25. G. M. O'regan, P. M. J. H. Kemperman, A. Sandilands, H. Chen, L. E. Campbell, K. Kroboth, R. Watson, M. Rowland, G. J. Puppels, W. H. I. McLean, P. J. Caspers, A. D. Irvine, Raman profiles of the stratum corneum define 3 filaggrin genotype–determined atopic dermatitis endophenotypes. *J. Allergy Clin. Immunol.* **126**, 574–580.e1 (2010).
26. C.-R. Kong, I. Barman, N. C. Dingari, J. W. Kang, L. Galindo, R. R. Dasari, M. S. Feld, A novel non-imaging optics based Raman spectroscopy device for transdermal blood analyte measurement. *AIP Adv.* **1**, 032175 (2011).
27. J. Lipson, J. Bernhardt, U. Block, W. R. Freeman, R. Hofmeister, M. Hristakeva, T. Lenosky, R. McNamara, D. Petrasek, D. Veltkamp, S. Waydo, *Requirements for Calibration in Noninvasive Glucose Monitoring by Raman Spectroscopy* (SAGE Publications, 2009).
28. N. C. Dingari, I. Barman, G. P. Singh, J. W. Kang, R. R. Dasari, M. S. Feld, Investigation of the specificity of Raman spectroscopy in non-invasive blood glucose measurements. *Anal. Bioanal. Chem.* **400**, 2871–2880 (2011).
29. I. Barman, C.-R. Kong, G. P. Singh, R. R. Dasari, Effect of photobleaching on calibration model development in biological Raman spectroscopy. *J. Biomed. Opt.* **16**, 011004 (2011).
30. I. Barman, N. C. Dingari, G. P. Singh, J. S. Soares, R. R. Dasari, J. M. Smulko, Investigation of noise-induced instabilities in quantitative biological spectroscopy and its implications for noninvasive glucose monitoring. *Anal. Chem.* **84**, 8149–8156 (2012).
31. H. J. Butler, L. Ashton, B. Bird, G. Cinque, K. Curtis, J. Dorney, K. Esmonde-White, N. J. Fullwood, B. Gardner, P. L. Martin-Hirsch, M. J. Walsh, M. R. McAinsh, N. Stone, F. L. Martin, Using Raman spectroscopy to characterize biological materials. *Nat. Protoc.* **11**, 664–687 (2016).

32. C.-R. Kong, thesis, Massachusetts Institute of Technology (2011).
33. K. De Gussem, J. De Gelder, P. Vandenabeele, L. Moens, The Biodata toolbox for MATLAB. *Chemom. Intell. Lab. Syst.* **95**, 49–52 (2009).
34. W.-C. Shih, K. L. Bechtel, M. V. Rebec, Noninvasive glucose sensing by transcutaneous Raman spectroscopy. *J. Biomed. Opt.* **20**, 051036 (2015).
35. S. P. Singh, S. Mukherjee, L. H. Galindo, P. T. C. So, R. R. Dasari, U. Z. Khan, R. Kannan, A. Upendran, J. W. Kang, Evaluation of accuracy dependence of Raman spectroscopic models on the ratio of calibration and validation points for non-invasive glucose sensing. *Anal. Bioanal. Chem.* **410**, 6469–6475 (2018).
36. A. Shrivastava, V. B. Gupta, Methods for the determination of limit of detection and limit of quantitation of the analytical methods. *Chron.Young Sci.* **2**, 21–25 (2011).
37. N. Li, H. Zang, H. Sun, X. Jiao, K. Wang, T. C.-Y. Liu, Y. Meng, A noninvasive accurate measurement of blood glucose levels with raman spectroscopy of blood in microvessels. *Molecules* **24**, E1500 (2019).
38. S. J. Orfanidis, *Introduction to Signal Processing* (Prentice-Hall Inc., 1995).
39. J. Zhao, H. Lui, D. I. McLean, H. Zeng, Automated autofluorescence background subtraction algorithm for biomedical Raman spectroscopy. *Appl. Spectrosc.* **61**, 1225–1232 (2007).
40. S. Wang, J. Zhao, H. Lui, Q. He, J. Bai, H. Zeng, Monte Carlo simulation of in vivo Raman spectral measurements of human skin with a multi-layered tissue optical model. *J. Biophotonics* **7**, 703–712 (2014).

Acknowledgments: J.W.K. thanks H. Yoon for helping with animal experiments and M. Jamiel and J. Haupt from MIT Division of Comparative Medicine for animal handling during the experiments. **Funding:** This work was supported by NIH (5P41EB15871, National Institute of Biomedical Imaging and Bioengineering) and Samsung Advanced Institute of Technology (Suwon, South Korea). P.T.C.S. acknowledges support from U01-NS090438-03, R21-NS105070-01, R01-HL121386-03, the Singapore-MIT Alliance 2 (Cambridge, MA, USA), the BioSym IRG of Singapore-MIT Alliance Research and Technology Center (Cambridge, MA, USA), and Hamamatsu Corporation (Hamamatsu City, Japan). **Author contributions:** J.W.K. designed and performed experiments, analyzed the result, and wrote the manuscript. Y.S.P. and W.L. analyzed the result and wrote the manuscript. H.C. performed experiments, led ray-tracing simulation, and wrote the manuscript. S.P.S. performed experiments, analyzed the result, and wrote the manuscript. W.C. designed the optical fiber probe, and L.H.G. fabricated the designed probe. R.R.D. and J.P. made intellectual contributions to the project. S.H.N. and P.T.C.S. supervised the study, coordinated the researchers, and wrote the manuscript. **Competing interests:** J.W.K. and P.T.C.S. are inventors on a patent application related to this work filed by Massachusetts Institute of Technology (US 62/893902, 30 August 2019). Y.S.P., H.C., W.L., and/or S.H.N. are inventors on three patent applications related to this work filed by Samsung Electronics Co. Ltd. (US16/172279, 26 October 2018; US16/297153, 8 March 2019; US16/527983, 31 July 2019). Y.S.P., H.C., W.L., S.H.N., and J.P. are employed by Samsung Electronics Co. Ltd. The authors declare no other competing interests. **Data and materials availability:** All data needed to evaluate the conclusions in the paper are present in the paper and/or the Supplementary Materials. Additional data related to this paper may be requested from the authors.

Submitted 29 June 2019
Accepted 20 November 2019
Published 24 January 2020
10.1126/sciadv.aay5206

Citation: J. W. Kang, Y. S. Park, H. Chang, W. Lee, S. P. Singh, W. Choi, L. H. Galindo, R. R. Dasari, S. H. Nam, J. Park, P. T. C. So, Direct observation of glucose fingerprint using in vivo Raman spectroscopy. *Sci. Adv.* **6**, eaay5206 (2020).